Molecular Electrochemistry Hot Paper Probing the Activity of Iron Peroxo Porphyrin Intermediates in the Reaction Layer during the Electrochemical Reductive Activation of O2

Jean-Marc Noel, Nikolaos Kostopoulos, Célia Achaibou, Claire Fave, Elodie Anxolabéhère-Mallart, Frédéric Kanoufi

▶ **To cite this version:**

Jean-Marc Noel, Nikolaos Kostopoulos, Célia Achaibou, Claire Fave, Elodie Anxolabéhère-Mallart, et al.. Molecular Electrochemistry Hot Paper Probing the Activity of Iron Peroxo Porphyrin Intermediates in the Reaction Layer during the Electrochemical Reductive Activation of O2. Angewandte Chemie International Edition, 2020, 59 (38), pp.16376-16380. hal-02951626

HAL Id: hal-02951626

https://u-paris.hal.science/hal-02951626

Submitted on 28 Sep 2020

HAL is a multi-disciplinary open access archive for the deposit and dissemination of scientific research documents, whether they are published or not. The documents may come from teaching and research institutions in France or abroad, or from public or private research centers.

L'archive ouverte pluridisciplinaire **HAL**, est destinée au dépôt et à la diffusion de documents scientifiques de niveau recherche, publiés ou non, émanant des établissements d'enseignement et de recherche français ou étrangers, des laboratoires publics ou privés.

Check for updates

Molecular Electrochemistry Hot Paper

Zitierweise:
Internationale Ausgabe: doi.org/10.1002/anie.202004977
Deutsche Ausgabe: doi.org/10.1002/ange.202004977

Probing the Activity of Iron Peroxo Porphyrin Intermediates in the Reaction Layer during the Electrochemical Reductive Activation of O_2

Jean-Marc Noel, Nikolaos Kostopoulos, Célia Achaibou, Claire Fave, Elodie Anxolabéhère-Mallart,* and Frédéric Kanoufi**

Abstract: *Herein we report the first example of using scanning electrochemical microscopy (SECM) to quantitatively analyze O_2 reductive activation in organic media catalyzed by three different Fe porphyrins. For each porphyrin, SECM can provide in one single experiment the redox potential of various intermediates, the association constant of Fe^{II} with O_2, and the pK_a of the $Fe^{III}(OOH^-)$/ $Fe^{III}(OO^{2-})$ couple. The results obtained can contribute to a further understanding of the parameters controlling the catalytic efficiency of the Fe porphyrin towards O_2 activation and reduction.*

Oxidations are an important class of reactions in the chemical industry for the production of huge quantities of intermediate and final products. In the current economic and environmental context, the ideal oxidant is O_2 as it is abundant and benign (H_2O as by-product).[1] In nature, this O_2 activation is achieved through the so-called reductive activation and corresponds to a partial and controlled reduction of O_2 bound at a metal active site via sequential e^- and H^+ transfers. Cleavage of the O–O bond generates the reactive high-valent oxygen species. O_2 activation under mild conditions using earth-abundant-metal catalysts has thus become a major focus in heterogeneous, homogeneous, and biological catalysis.[2]

The use of Fe porphyrins (Figure 1 A) is an interesting biomimetic approach for O_2 activation, as Fe^{II} can reproduce the metabolic transformation catalyzed by Fe enzymes such as CytP450.[3,4] The first step of the catalytic cycle is the binding of O_2 to Fe^{II} to form an $Fe^{III}(OO^{\bullet-})$ (superoxo) intermediate which can be ultimately reduced to a $Fe^{III}(OO^{2-})$ (peroxo) intermediate (Figure 2 A). Due to their transient character, the isolation and spectroscopic characterization of such metal-bound reactive oxygen intermediates usually relies on their chemical generation and cryogenic trapping.[5] In the case of O_2 electrochemical activation, owing to the binding of the different O_2 reactive species at the metal active center, Fe porphyrins act as inner-sphere homogeneous catalysts, meaning that they serve as an electron shuttle (or a redox mediator) between the electrode and the metal-bound O_2 species.[6] Efficient electrocatalysis then engages the reactive intermediates in a thin layer adjacent the electrode, which impedes the direct observation of their (electro)chemical reactivity. Henceforth, the rational benchmarking of electrocatalysts, relying on structure–activity relationships regarding the formation or activity of such intermediates, is mostly based on thermodynamic arguments and at best DFT computations.[7]

Scanning electrochemical microscopy (SECM) offers an elegant approach to capture, quantify, and characterize short-lived intermediates,[8,9] including those in complex molecular homogeneous catalytic systems.[9] Here, the substrate generation–tip collection (SG/TC) mode is employed, as shown in Figure 1 B and detailed in Section 1 of the Supporting Information, SI. Briefly, the SECM is mounted inside a glove bag, allowing a controlled O_2 or Ar atmosphere and minimizing water contamination. A macroelectrode (a glassy carbon generator, G) is used to activate O_2 reduction by Fe porphyrin. The porphyrin in the Fe^{III} state, is reduced at G,

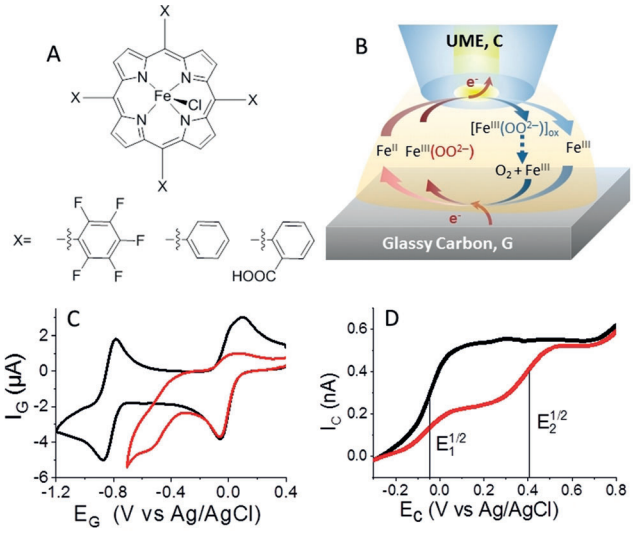

Figure 1. A) Various Fe porphyrins used in this work: $Fe^{III}(F_{20}TPP)Cl$, $Fe^{III}(TPP)Cl$, $Fe^{III}((2\text{-}CO_2H)_4TPP)Cl$; B) Setup used for a typical SECM investigation in the SG/TC mode of O_2 activation by Fe porphyrins. C) CVs recorded at GC electrode (G, 3 mm diameter) at $\nu = 0.1\ V s^{-1}$ and D) LSVs recorded at a gold UME (C, 25 µm diameter) at $\nu = 20\ mV s^{-1}$, in SG/TC mode, held at $d = 8 \pm 2$ µm from G, polarized at $E_C = -0.7$ V vs. Ag/AgCl, in DMF 0.1 M $TBAPF_6$ with 0.5 mM $[(FeF_{20}TPP)Cl]$ under argon (black trace) and with 1 mM O_2 (red trace).

[*] Dr. J.-M. Noel, Dr. F. Kanoufi
Université de Paris, ITODYS, CNRS
75006 Paris (France)
E-mail: jean-marc.noel@univ-paris-diderot.fr
frederic.kanoufi@univ-paris-diderot.fr
N. Kostopoulos, Dr. C. Achaibou, Dr. C. Fave,
Dr. E. Anxolabéhère-Mallart
Université de Paris, Laboratoire d'Electrochimie Moléculaire, CNRS
75006 Paris (France)
E-mail: elodie.anxolabehere@univ-paris-diderot.fr
Supporting information and the ORCID identification number(s) for the author(s) of this article can be found under: https://doi.org/10.1002/anie.202004977.

© 2020 Wiley-VCH Verlag GmbH & Co. KGaA, Weinheim

while, simultaneously the electrogenerated intermediates are collected that is, reoxidized at a 25 μm gold UME tip (collector, C) at controlled distance from G.

The activation of O_2 by Fe porphyrin had been previously studied in generation–collection configurations; however, this was mostly limited to the probing of final products (H_2O_2) at ring-disk electrodes.[10] SECM offers higher collection efficiency, at smaller and controllable generator–collector gap separation.[11] In the case SECM studies of porphyrin, surface charge transfer rates have been probed[12] and, during O_2 reduction, only final products have been detected.[13] Here it will allow deeper mechanistic insights through the real-time in situ probing of the metal-oxo intermediates formed during O_2 activation.

We focus here on the first intermediate produced in non-acidic medium, the $Fe^{III}(OO^{2-})$ (peroxo) adduct, for three porphyrins showing, based on earlier work,[7,14] different electronic density ($Fe(F_{20}TPP)Cl$, Fe(TPP)Cl, and $Fe((2\text{-}CO_2H)_4TPP)Cl$). New thermodynamic and kinetic parameters are experimentally obtained and related to earlier DFT calculations. This information, obtained in the absence of H^+, is then related to the efficiency of these catalysts for O_2 reduction in the presence of H^+.

Cyclic voltammograms (CVs) at G, for the reduction of $[(Fe^{III}F_{20}TPP)Cl]$ obtained under Ar and O_2, are shown in Figure 1C. Under Ar (black trace), the CV exhibits two successive reversible reductions steps: Fe^{III}/Fe^{II} with $E^0_{Fe^{III}/Fe^{II}} = -0.08$ V and Fe^{II}/Fe^{I} with $E^0_{Fe^{II}/Fe^{I}} = -0.9$ V. After introduction of O_2 in the solution (red trace), a new irreversible reduction, slightly less cathodic than the $O_2/O_2^{\bullet-}$ feature, appeared at $E^p_{Fe^{III}(OO^{\bullet-})/Fe^{III}(OO^{2-})} \approx -0.6$ V. In the absence of H^+, it is assigned to the reduction of the end-on superoxo adduct $Fe^{III}(OO^{\bullet-})$ into a side-on peroxo $Fe^{III}(OO^{2-})$. Indeed, upon reduction, significant electronic reshuffling occurs as well as a change of the coordination mode of the O_2 ligand from end-on to side-on.[5a,d,14]

In order to probe the reactivity of these Fe porphyrin–O_2 intermediates, SECM SG/TC experiments were performed holding the potential of G at $E_G = -0.7$ V, while sweeping anodically, in a LSV curve, the UME potential, E_C. Under Ar, the LSV at C probes a single oxidation event at the half-wave potential $E^{1/2}_{1,C} \approx -0.05$ V, attesting to the collection of Fe^{II} (black trace, Figure 1D). Under O_2, the LSV at C (red trace, Figure 1D) presents an additional second oxidation wave at $E^{1/2}_{2,C} \approx 0.4$ V. This new wave is attributed to the oxidation of $Fe^{III}(OO^{2-})$ probed directly in the diffusion layer of G corroborating its relative stability.[14] First, the absence of a collection current at the SECM tip for E_C close to $E^p_{Fe^{III}(OO^{\bullet-})/Fe^{III}(OO^{2-})}$ indicates that the reoxidation of $Fe^{III}(OO^{2-})$ does not yield $Fe^{III}(OO^{\bullet-})$, likely owing to the change in O_2 coordination within the porphyrin complex during the electron transfer steps.[5a,d,14] As a consequence, the $Fe^{III}(OO^{\bullet-})/Fe^{III}(OO^{2-})$ couple does not behave here as a reversible system, except at low temperature (210 K).[5d] Instead the oxidation of $Fe^{III}(OO^{2-})$ produces a different species, namely $Fe^{III}(OO^{2-})_{ox}$ at a much more anodic potential ca. 0.4 V than that at which it is generated. Hence, the formation and oxidation of $Fe^{III}(OO^{2-})$ involve two different irreversible redox couples, that is, $Fe^{III}(OO^{\bullet-})/Fe^{III}(OO^{2-})$ and $Fe^{III}(OO^{2-})_{ox}/Fe^{III}(OO^{2-})$; the former reductive formation is located at ca. −0.6 V while the latter oxidation is located at ca. 0.4 V.

Interestingly, under O_2, the sum of the current contributions corresponding to the oxidative collection of Fe^{II}, $I_{Fe^{II}}$, and to that of $Fe^{III}(OO^{2-})$, $I_{Fe^{III}(OO^{2-})}$, matches the current plateau for Fe^{II} collection under Ar (Figure 1D). The conservation of the faradaic balance suggests $Fe^{III}(OO^{2-})$ is oxidized at C, in a one-electron exchange, into $[Fe^{III}(OO^{2-})]_{ox}$ (Figure 2A), which dissociates to a Fe^{III}, maintaining the feedback loop at G. The decrease of $I_{Fe^{II}}$ at C agrees qualitatively with the loss of reversibility on the oxidation of Fe^{II} to Fe^{III} observed on the CV at G (Figure 1C).

Thin-layer UV/Vis spectroelectrochemistry experiments show that in a solution of electrochemically generated $Fe^{III}(OO^{2-})$, if a potential of 0.6 V is applied, a spectral signature similar to that of the starting Fe^{III} species appears (see SI, Section 2). We propose that the oxidation of the species is followed by chemical decomposition possibly by release of O_2 as suggested by the oxidation of chemically prepared non-heme $Fe^{III}(OO^{2-})$.[15] The SECM experiments corroborate a similar reaction scheme.

The relevance of the SECM probing of this reaction path was tested with COMSOL® simulations (see SI, Section 3). In the absence of a proton source, the simplified reaction scheme in Figure 2A was simulated. The irreversible reductive formation of $Fe^{III}(OO^{2-})$ and its irreversible oxidation are characterized by two different formal potentials, E^0_2 and E^0_3 ($E^0_2 < E^0_3$). The model also considers 1) the association between O_2 and Fe^{II} described by the equilibrium constant K_{O_2}, and 2) the chemical stability of the peroxo derivative, $Fe^{III}(OO^{2-})$, through a first-order decomposition rate constant, k_d. The first-order nature of k_d is confirmed spectroelectrochemically (see Figure S2C, SI). The influence of both parameters on the simulated LSVs at G and C is presented in Figure 2B–E.

In Figure 2B, the higher K_{O_2}, the higher and less cathodic the reduction peak of $Fe^{III}(OO^{\bullet-})$ is at G. Meanwhile at C, increasing K_{O_2} results in a drop of the collection of Fe^{II}, $I_{Fe^{II}}$ in favor of that of $Fe^{III}(OO^{2-})$, $I_{Fe^{III}(OO^{2-})}$ (overall decrease of the ratio $I_{Fe^{II}}/I_{Fe^{III}(OO^{2-})}$). Noteworthy, even for weak binding ($K_{O_2} < 1\,M^{-1}$) the $Fe^{III}(OO^{2-})$ intermediate could be collected at C, whereas its formation cannot be detected at G. Conversely for strong binding ($K_{O_2} > 100\,M^{-1}$) only $Fe^{III}(OO^{2-})$ is collected at C (though distance dependent) whereas the feature corresponding to the reduction of $Fe^{III}(OO^{\bullet-})$ to $Fe^{III}(OO^{2-})$ at G is still affected by K_{O_2}. However, absolute determination of K_{O_2} only from the LSV curves at G is delicate. It indeed requires prior knowledge about the $Fe^{III}(OO^{\bullet-})$ E^0 and is subject to baseline correction uncertainties owing to the nearby $O_2/O_2^{\bullet-}$ reduction feature (see the LSV in Figure 3). Figure 2B,C suggests the dual G and C responses remove such uncertainties.

The complexity in the mechanistic determination is further stressed by the chemical instability of the peroxo derivative, $Fe^{III}(OO^{2-})$. Thin-layer UV/Vis spectroelectrochemistry (Section 2, SI) revealed that the electrogenerated $Fe^{III}(OO^{2-})$ complex decomposes with time into Fe^{III}. This evolution was modeled by the rate constant k_d, (arrows

 © 2020 Wiley-VCH Verlag GmbH & Co. KGaA, Weinheim

These are not the final page numbers!

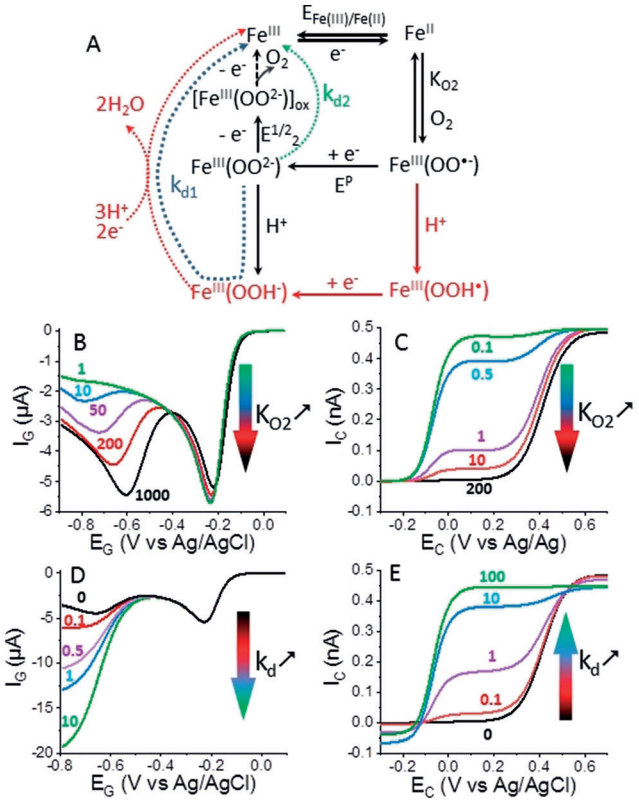

Figure 2. A) Mechanistic scheme: the black and green (k_{d2}) or blue (k_{d1}) parts correspond to the reaction cycle used for the simulations (see Section 3, SI,) whereas the red pathway (involving H^+) is related to the TOF of the $4e^-/4H^+$ reduction of O_2 to water determined in acidic medium. B–E) Influence of K_{O_2} and k_d on the simulated LSV curves at G (B, D) and at C in the SG/TC mode, $d = 8$ μm, (C, E) using parameters defined in Table S1, SI. B,C) $k_d = 0\ s^{-1}$ and B) $K_{O_2} = 1$–$1000\ M^{-1}$ and C) $K_{O_2} = 0.1$–$200\ M^{-1}$ from top to bottom. D,E) $K_{O_2} = 200\ M^{-1}$ and D) $k_d = 0$–$100\ s^{-1}$ from top to bottom and E) $k_d = 0$–$10\ s^{-1}$ from bottom to top.

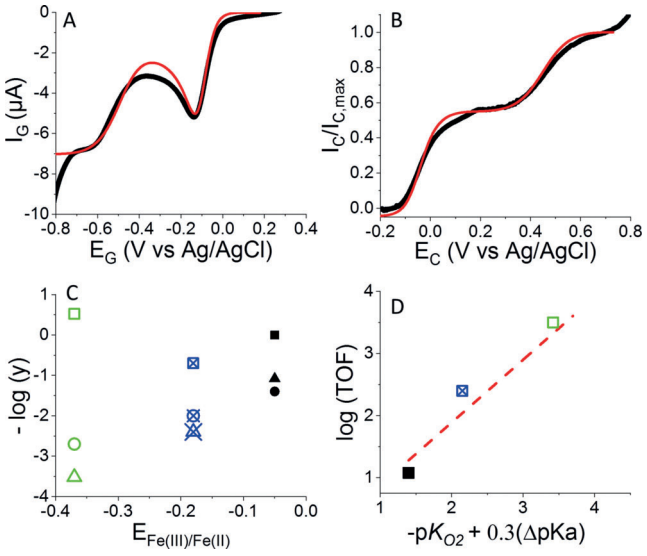

Figure 3. A) LSVs recorded at G and B) the dimensionless LSVs obtained subsequently at C and at a scan rate of 50 $mV s^{-1}$ in the SG/TC mode at $d = 8 \pm 2$ μm from G held at $E_G = -0.7$ V in 0.1 M $TBAPF_6$/DMF in the presence of 1 mM O_2 and 0.5 mM [($Fe^{III}F_{20}TPP$)Cl. Red lines are the corresponding simulated LSVs using $K_{O_2} = 25\ M^{-1}$ and $k_d = 1\ s^{-1}$. C) −log(γ), γ being k_d (■), K_{O_2} (●) and the TOF (▲) plotted versus $E^0_{Fe^{III}/Fe^{II}}$. D) Testing Eq. (1) for log (TOF) variations. Black solid, blue crossed, and green open symbols correspond to $Fe^{III}(F_{20}TPP)Cl$, $Fe^{III}(TPP)Cl$, and $Fe^{III}((2\text{-}CO_2H)_4TPP)Cl$, respectively.

labeled k_{d1} and k_{d2} in Figure 2 A). The simulated curves in Figure 2 D,E show the effect of k_d on the LSV at G and at C, respectively. At G, the superoxo reduction current in a catalytic fashion increases with higher k_d. Conversely, at C, Fe^{II} tends to be the predominant species (increase of $I_{Fe^{II}}/I_{Fe^{III}(OO^{2-})}$). Noteworthy, for $k_d = 100\ s^{-1}$ a small amount of $Fe^{III}(OO^{2-})$ can still be collected at C, meaning that in principle an intermediate species with a lifetime as low as 10 ms could be probed for the given UME size and G–C gap.

The opposite trends observed at C for K_{O_2} (decrease of $I_{Fe^{II}}/I_{Fe^{III}(OO^{2-})}$) and k_d (increase of $I_{Fe^{II}}/I_{Fe^{III}(OO^{2-})}$), combined with the LSV at G, allow K_{O_2} and k_d to be unequivocally determined from the fit of the LSVs at G and C. This strategy (Section 4, SI) is used to describe the activation of O_2 by three iron porphyrins. The main results obtained with the three porphyrins are summarized in Table 1.

The best fit of the experimental LSVs at G and the C UME for $Fe(F_{20}TPP)$ is obtained for $K_{O_2} = 25 \pm 10\ s^{-1}$, a value comparable but lower to previous estimate based only on the analysis of the CVs at G (see Section 4, SI),[14] and $k_d = 1 \pm 0.3\ s^{-1}$ as shown in Figure 3 A,B. k_d is 20 times higher than the apparent $Fe^{III}(OO^{2-})$ decomposition rate constant determined by the thin-layer spectroelectrochemical study at 253 K (Section 2, SI), a difference that could be accounted for by the 40 K temperature difference between the two experiments.

It is then extended to [$Fe^{III}(TPP)Cl$] and [$Fe^{III}((2\text{-}CO_2H)_4TPP)Cl$]. The LSVs recorded under O_2 at G for each porphyrin are shown in Figure S4-2 A,C. The change in $E^0_{Fe^{III}/Fe^{II}}$ toward more cathodic values (−0.18 and −0.37 V, respectively) when changing the phenyl rings substituents agrees with previous studies[7] and results from an increase in the electron density of the ligand, while it has little effect on the peak potential for $Fe^{III}(OO^{\bullet-})$ reduction:

Table 1: Redox potentials of catalysts and intermediates [V vs. Ag/AgCl], TOFs, association constants (K_{O_2}), and apparent dissociation rate constants of $Fe^{III}(OO^{2-})$ (k_d). The errors on the potentials were estimated based on three or four different experiments for each porphyrin.

Catalyst	$E^0_{Fe^{III}/Fe^{II}}$	$E^p_{[Fe^{III}(OO^{\bullet-})]/[Fe^{III}(OO^{2-})]}$	$E^{1/2}_{[[Fe^{III}(OO^{2-})]_{ox}]/[Fe^{III}(OO^{2-})]}$	TOF [s^{-1}]	K_{O_2} [M^{-1}]	k_d [s^{-1}]
$Fe^{III}(Fe_{20}TPP)Cl$	-0.05 ± 0.03	-0.58 ± 0.05	0.39 ± 0.04	12	25 ± 10	1 ± 0.3
$Fe^{III}(TPP)Cl$	-0.18 ± 0.01	-0.64 ± 0.01	0.18 ± 0.03	250	100 ± 40	5 ± 1
$Fe^{III}((2\text{-}CO_2H)_4TPP)Cl$	-0.37 ± 0.02	-0.62 ± 0.02	-0.07 ± 0.03	3300	500 ± 100	0.3 ± 0.1

© 2020 Wiley-VCH Verlag GmbH & Co. KGaA, Weinheim

$E^{p}_{Fe^{III}(OO^{\bullet-})/Fe^{III}(OO^{2-})} \approx -0.6$ V. The already reported[7] donating effect of the 2-COOH substituents is likely due to intraligand hydrogen-bond effects, which are expected to lower the COOH pK_a,[16] henceforth conferring it an +I effect.

On the LSVs recorded at C while the solution was electrolyzed at G ($E_G = -0.7$ V, Figure S4-2 B,D), two steps are probed and attributed, like for $Fe^{III}(F_{20}TPP)$, to the oxidation of Fe^{II} and $Fe^{III}(OO^{2-})$ (with $E^{1/2}_{[Fe^{III}(OO^{2-})]_{ox}/Fe^{III}(OO^{2-})} \approx 0.2$ and -0.05 V, respectively). K_{O_2} and k_d values were also extracted from the fit of the G and C LSVs. Noteworthy, the K_{O_2} value determined for $[Fe^{III}(TPP)Cl]$ is in excellent agreement with the DFT-calculated value,[7] strengthening the proposed methodology for accurately estimating the association constant K_{O_2}.

The experimental determination of K_{O_2} and k_d, as well as the reduction/oxidation potentials of new intermediates, provides access to structure–activity correlations within the iron porphyrin series. They are presented, in a logarithmic scale, in Figure 3 A relative to $E^0_{Fe^{III}/Fe^{II}}$. $\log(K_{O_2})$ varies linearly with $E^0_{Fe^{III}/Fe^{II}}$ with a slope of 60 mV per K_{O_2} decade, confirming experimentally the DFT-observed trend.[7] This shows in first instance the effect of decreasing ligand electron density which shifts $E^0_{Fe^{III}/Fe^{II}}$ to more positive values and lowers affinity to O_2.

In contrast, this decrease of ligand electron density should improve the stabilization of the reduced adduct ($Fe^{III}(OO^{2-})$) and should be reflected through either its stability rate constant k_d or the $Fe^{III}(OO^{\bullet-})$ reduction and $Fe^{III}(OO^{2-})$ oxidation potentials. If the latter ($E^{1/2}_{[Fe^{III}(OO^{2-})]_{ox}/Fe^{III}(OO^{2-})}$ determined at C for each porphyrin) varies linearly with $E^0_{Fe^{III}/Fe^{II}}$ with near-unity slope (Figure S5, Section 5, SI), there is a deviation for the other two.

Firstly, k_d should increase from $[Fe^{III}(F_{20}TPP)Cl]$ to $[Fe^{III}((2\text{-}CO_2H)_4TPP)Cl]$. If the trend is followed for $[Fe^{III}(F_{20}TPP)Cl]$ and $[Fe^{III}(TPP)Cl]$, the lowest k_d value was obtained for $[Fe^{III}((2\text{-}CO_2H)_4TPP)Cl]$, likely due to H-bond stabilization.

The $E^{1/2}_{[Fe^{III}(OO^{2-})]_{ox}/Fe^{III}(OO^{2-})} - E^0_{Fe^{III}/Fe^{II}}$ correlation suggests that electron transfer from the electrode to the Fe-O intermediates is controlled by the electron density of the porphyrin ligand, in agreement with the redox-mediating role of Fe porphyrin. From this argument one would expect that $E^{p}_{Fe^{III}(OO^{\bullet-})/Fe^{III}(OO^{2-})}$ shifts toward more cathodic potentials, as $E^0_{Fe^{III}/Fe^{II}}$ when the ligand electron density is increased. The relative insensitivity of $E^{p}_{Fe^{III}(OO^{\bullet-})/Fe^{III}(OO^{2-})}$ to the porphyrin ligand structure provides further mechanistic information. As shown from the simulated LSVs in Figure 2 B, increasing K_{O_2} also increases $E^{p}_{Fe^{III}(OO^{\bullet-})/Fe^{III}(OO^{2-})}$ by ca. 90 mV per K_{O_2} decade. However, considering the possible correlation $E^{p}_{Fe^{III}(OO^{\bullet-})/Fe^{III}(OO^{2-})} = E^0_{Fe^{III}/Fe^{II}} - 0.09\,pK_{O_2} + B$, where B is a constant term within the porphyrin series including standard potential differences between the two reductive steps $\Delta E^0 = E^0_{Fe^{III}/Fe^{II}} - E^0_{Fe^{III}(OO^{\bullet-})/Fe^{III}(OO^{2-})}$, a deviation from a unity slope is found (Section 6, SI). It means that K_{O_2} is not sufficient to explain the potential shift. Indeed owing to its stronger basic character, the electrogeneration of $Fe^{III}(OO^{2-})$ should be influenced by protonation (for example by residual water in the absence of added acid), which depends on the ligand porphyrin structure. As a first guess this protonation should be related to the pK_a of $Fe^{III}(OOH^-)/Fe^{III}(OO^{2-})$ and affect the LSV through an apparent E^0 varying as $E^0_{Fe^{III}(OO^{\bullet-})/Fe^{III}(OO^{2-})} + 0.06\,pK_a$. Thus, one expects $E^{p}_{Fe^{III}(OO^{\bullet-})/Fe^{III}(OO^{2-})} = E^0_{Fe^{III}/Fe^{II}} + 0.06\,pK_a - 0.09\,pK_{O_2} + B'$, where B' is a constant term along the porphyrin series. A ΔpK_a scale relative to the pK_a of $[Fe^{III}(F_{20}TPP)Cl]$, $\Delta pK_a = pK_a - pK_{aFeF_{20}TPP}$ as explained in Section S6, SI, can be evaluated experimentally (Figure S6). It yields $\Delta pK_a = 0.4$ for $[Fe^{III}(TPP)Cl]$ and $\Delta pK_a = 2.6$ for $[Fe^{III}((2\text{-}CO_2H)_4TPP)Cl]$. These values match the trend in ΔpK_a estimated by DFT within the parallel protonation of the superoxo couple $Fe^{III}(OOH^{\bullet})/Fe^{III}(OO^{\bullet-})$ (red path Figure 2 A).[7] It then suggests that the structure affects similarly the $Fe^{III}(OOH^-)/Fe^{III}(OO^{2-})$ and $Fe^{III}(OOH^{\bullet})/Fe^{III}(OO^{\bullet-})$ pK_as.

Both protonation steps are key in the tuning of the turnover catalytic frequency (TOF) during the electrochemical reduction of O_2, the prominence of each depending on the strength of the acid used. Thus the TOF for the electrochemical reduction of O_2 in acidic medium was determined for each porphyrin from the foot of the wave analysis (FOWA) as described by Savéant et al. (see Section 7, SI).[17] The TOF values found for the three porphyrins are slightly higher but on the same order of magnitude as the values reported for porphyrins having similar $E^0_{Fe^{III}/Fe^{II}}$, probably due to the higher dissociation of $HClO_4$ in DMF. Both log(TOF) and $\log(K_{O_2})$ vary linearly with $E^0_{Fe^{III}/Fe^{II}}$, showing a direct relationship between the catalytic efficiency and the O_2 binding. In order to predict the TOF of catalysts, it was shown, from transition state arguments and DFT estimates, that log(TOF) varies linearly with pK_{O_2} and the $Fe^{III}(OOH^{\bullet})/Fe^{III}(OO^{\bullet-})$ pK_a.[7] Considering the abovementioned similar structure effect on the pK_as of $Fe^{III}(OOH^{\bullet})/Fe^{III}(OO^{\bullet-})$ and $Fe^{III}(OOH^-)/Fe^{III}(OO^{2-})$, one then expects a similar trend [Eq. (1)],

$$\log(TOF) = -pK_{O_2} + \alpha\, pK_{a,Fe^{III}(OOH^-)/Fe^{III}(OO^{2-})} + B'' \quad (1)$$

where B'' is a constant term within the series. This relationship is indeed verified here, in Figure 3 D, but with experimentally estimated thermodynamic parameters and using $\alpha = 0.3$, a value very similar to that obtained correlating TOF and the DFT-estimated $Fe^{III}(OOH^{\bullet})/Fe^{III}(OO^{\bullet-})$ pK_as.[7]

To summarize, we have demonstrated here all the potentiality of SECM in the SG/TC mode to decipher complex homogeneous catalytic systems based on the in situ probing of reaction intermediates. Particularly, with the help of simulations, we could quantitatively extract for the first time thermodynamic and kinetic parameters for such intermediates of complex processes in a single electrochemical experiment. It is exemplified here for probing the reductive activation of O_2 by iron porphyrins. Even in the absence of acid, the activity of intermediate oxo adducts, collected at the tip of a SECM, make it possible to draw pertinent structure–activity correlations to address the catalysis of O_2 reduction by such catalysts. The importance of O_2 binding and the peroxo protonation is highlighted through experimental estimates that correlate with catalysis TOF and earlier DFT calculations.[7] Moreover, in the absence of H^+, a decomposi-

 © 2020 Wiley-VCH Verlag GmbH & Co. KGaA, Weinheim

These are not the final page numbers!

tion path (k_d) of the peroxo intermediates has been evidenced. At that point, two mechanistic paths can be envisaged 1) $k_{d,1}$ is associated with the protonation of $Fe^{III}(OO^{2-})$ and participates in the TOF as it engages the two-electron reduction process of the $Fe^{III}OOH$ (dashed blue arrow in Figure 2A) and 2) $k_{d,2}$ is a concurrent path to the TOF (dashed green arrow), which, as suggested from the spectroelectrochemical experiments, corresponds to the homogeneous dissociation of peroxo. Even if its real effect is not clear, it raises interesting questions with implications for the catalytic process.

Finally, the determination by SECM of the exact location of the oxidation process opens electrochemical access to new highly oxidative intermediates. Particularly the increased interest in nanoelectrodes will draw unique opportunities in probing more unstable intermediates within thinner reaction layers. The proof of concept established here with O_2 activation can also be transposed to other relevant cases such as CO_2 reduction.

Acknowledgements

We are grateful for financial support by Labex MiChem, managed by ANR, within the Investissement d'Avenir program under reference ANR-11-IDEX-004-02.

Conflict of interest

The authors declare no conflict of interest.

Keywords: electrocatalysis · iron porphyrins · molecular electrochemistry · O—O activation · scanning electrochemical microscopy

[1] F. Cavani, J. H. Teles, *ChemSusChem* **2009**, *2*, 508 – 534.
[2] a) E. I. Solomon, S. S. Stahl, *Chem. Rev.* **2018**, *118*, 2299 – 2301; b) W. Zhang, W. Lai, R. Cao, *Chem. Rev.* **2017**, *117*, 3717 – 3797.
[3] D. Mansuy, *C. R. Chim.* **2007**, *10*, 392 – 413.
[4] E. Anxolabéhère-Mallart, F. Banse, *Curr. Opin. Electrochem.* **2019**, *15*, 118 – 124.
[5] a) J. G. Liu, T. Ohta, S. Yamaguchi, T. Ogura, S. Sakamoto, Y. Maeda, Y. Naruta, *Angew. Chem. Int. Ed.* **2009**, *48*, 9262 – 9267; *Angew. Chem.* **2009**, *121*, 9426 – 9431; b) A. Takahashi, T. Kurahashi, H. Fujii, *Inorg. Chem.* **2011**, *50*, 6922 – 6928; c) X. Huang, J. T. Groves, *Chem. Rev.* **2018**, *118*, 2491 – 2553; d) H. Kim, P. J. Rogler, S. K. Sharma, A. W. Schaefer, E. I. Solomon, J. D. Karlin, *J. Am. Chem. Soc.* **2020**, *142*, 3104 – 3116.
[6] J.-M. Savéant, *Chem. Rev.* **2008**, *108*, 2348 – 2378.
[7] M. L. Pegis, B. A. McKeown, N. Kumar, K. Lang, D. J. Wasylenko, X. P. Zhang, S. Raugei, J. M. Mayer, *ACS Cent. Sci.* **2016**, *2*, 850 – 856.
[8] *Scanning Electrochemical Microscopy*, 2nd ed. (Eds.: A. J. Bard, M. V. Mirkin), CRC, Boca Raton, FL, **2012**.
[9] a) T. Kai, M. Zhou, S. Johnson, H. S. Ahn, A. J. Bard, *J. Am. Chem. Soc.* **2018**, *140*, 16178 – 16183; b) T. J. Stockmann, J. M. Noël, S. Ristori, C. Combellas, A. Abou-Hassan, F. Rossi, F. Kanoufi, *Anal. Chem.* **2015**, *87*, 9621 – 9630.
[10] a) C. T. Carver, B. D. Matson, J. M. Mayer, *J. Am. Chem. Soc.* **2012**, *134*, 5444 – 5447; b) C. Costentin, H. Dridi, J.-M. Savéant, *J. Am. Chem. Soc.* **2015**, *137*, 13535 – 13544; c) K. Sengupta, S. Chatterjee, A. Dey, *ACS Catal.* **2016**, *6*, 6838 – 6852.
[11] a) C. Sánchez-Sánchez, J. Rodríguez-López, A. J. Bard, *Anal. Chem.* **2008**, *80*, 3254 – 3260; b) S. Cannan, J. Cervera, R. J. Steliaros, E. Bitziou, A. L. Whitworth, P. R. Unwin, *Phys. Chem. Chem. Phys.* **2011**, *13*, 5403 – 5412.
[12] Y. Leroux, D. Schaming, L. Ruhlmann, P. Hapiot, *Langmuir* **2010**, *26*, 14983 – 14989.
[13] a) A. O. Okunola, T. C. Nagaiah, X. Chen, K. Eckhard, W. Schuhmann, M. Bron, *Electrochim. Acta* **2009**, *54*, 4971 – 4978; b) M. A. Mezour, R. Cornut, E. M. Hussien, M. Morin, J. Mauzeroll, *Langmuir* **2010**, *26*, 13000 – 13006.
[14] R. Oliveira, W. Zouari, C. Herrero, F. Banse, B. Schöllhorn, C. Fave, E. Anxolabéhère-Mallart, *Inorg. Chem.* **2016**, *55*, 12204 – 12210.
[15] S. Bang, Y. M. Lee, S. Hong, K. B. Cho, Y. Nishida, M. S. Seo, R. Sarangi, S. Fukuzumi, W. Nam, *Nat. Chem.* **2014**, *6*, 934 – 940.
[16] S. Shan, D. Herschlag, *J. Am. Chem. Soc.* **1996**, *118*, 5515 – 5518.
[17] C. Costentin, S. Drouet, M. Robert, J.-M. Saveant, *J. Am. Chem. Soc.* **2012**, *134*, 11235 – 11242.

Manuscript received: April 6, 2020
Accepted manuscript online: June 15, 2020
Version of record online: ■■ ■■, ■■■■

 © 2020 Wiley-VCH Verlag GmbH & Co. KGaA, Weinheim

Zuschriften

Molecular Electrochemistry

J.-M. Noel,* N. Kostopoulos,
C. Achaibou, C. Fave ——— ■■■■–■■■■

Probing the Activity of Iron Peroxo Porphyrin Intermediates in the Reaction Layer during the Electrochemical Reductive Activation of O_2

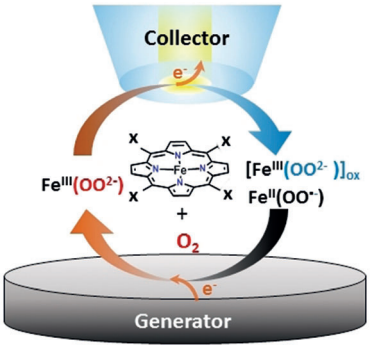

Catalysts in action: Scanning electrochemical microscopy was used to quantitatively analyze O_2 reductive activation in organic media catalyzed by three different Fe porphyrins. In one single experiment the redox potential of various intermediates, the association constant of Fe^{II} with O_2, and the pK_a of the Fe^{III}-(OOH^-)/ Fe^{III}(OO^{2-}) couple can be determined.

© 2020 Wiley-VCH Verlag GmbH & Co. KGaA, Weinheim

These are not the final page numbers!